

Article

Coagulated Mineral Adsorbents for Dye Removal, and Their Process Intensification Using an Agitated Tubular Reactor (ATR)

Alastair S. Tonge^{1,2,*}, David Harbottle¹ , Simon Casarin³, Monika Zervaki³ , Christel Careme³
and Timothy N. Hunter^{1,*} 

¹ School of Chemical and Process Engineering, University of Leeds, Leeds LS2 9JT, UK; d.harbottle@leeds.ac.uk

² United Utilities, Haweswater, Lingley Mere Business Park, Warrington WA5 3LP, UK

³ Imerys, 2 Place Edouard Bouillères, 31036 Toulouse, France; simon.casarin@imerys.com (S.C.); monika.zervaki@imerys.com (M.Z.); christel.careme@imerys.com (C.C.)

* Correspondence: alastair.tonge@uuplc.co.uk (A.S.T.); t.n.hunter@leeds.ac.uk (T.N.H.); Tel.: +44-113-343-2790 (T.N.H.)

Abstract: The aim of this study was to understand the efficacy of widely available minerals as dual-function adsorbents and weighter materials, for the removal of toxic azo-type textile dyes when combined with coprecipitation processes. Specifically, the adsorption of an anionic direct dye was measured on various mineral types with and without the secondary coagulation of iron hydroxide ('FeOOH') in both a bench-scale stirred tank, as well as an innovative agitated tubular reactor (ATR). Talc, calcite and modified bentonite were all able to remove 90–95% of the dye at 100 and 200 ppm concentrations, where the kinetics were fitted to a pseudo second-order rate model and adsorption was rapid (<30 min). Physical characterisation of the composite mineral-FeOOH sludges was also completed through particle size and sedimentation measurements, as well as elemental scanning electron microscopy to determine the homogeneity of the minerals in the coagulated structure. Removal of >99% of the dye was achieved for all the coagulated systems, where additionally, they produced significantly enhanced settling rates and bed compression. The greatest settling rate (9 mm min⁻¹) and solids content increase (450% *w/w*) were observed for the calcium carbonate system, which also displayed the most homogenous distribution. This system was selected for scale-up and benchmarking in the ATR. Dye removal and sediment dispersion in the ATR were enhanced with respect to the bench scale tests, although lower settling rates were observed due to the relatively high shear rate of the agitator. Overall, results highlight the applicability of these cost-effective minerals as both dye adsorbents and sludge separation modifiers to accelerate settling and compression in textile water treatment. Additionally, the work indicates the suitability of the ATR as a flexible, modular alternative to traditional stirred tank reactors.

Keywords: anionic azo dye; iron (oxy)hydroxide; coagulation; calcite; bentonite; talc



Citation: Tonge, A.S.; Harbottle, D.; Casarin, S.; Zervaki, M.; Careme, C.; Hunter, T.N. Coagulated Mineral Adsorbents for Dye Removal, and Their Process Intensification Using an Agitated Tubular Reactor (ATR). *ChemEngineering* **2021**, *5*, 35. <https://doi.org/10.3390/chemengineering5030035>

Academic Editor: Saeed Chehreh Chelgani

Received: 28 April 2021
Accepted: 1 July 2021
Published: 6 July 2021

Publisher's Note: MDPI stays neutral with regard to jurisdictional claims in published maps and institutional affiliations.



Copyright: © 2021 by the authors. Licensee MDPI, Basel, Switzerland. This article is an open access article distributed under the terms and conditions of the Creative Commons Attribution (CC BY) license (<https://creativecommons.org/licenses/by/4.0/>).

1. Introduction

Wastewater is generated in large amounts by the textile industry and may possess high colouration due to the presence of organic dyes that are not easily broken down through natural degradation [1]. Coloured water reduces light penetration that is required for the survival of aquatic organisms, and as such, textile effluents must be treated to remove dye compounds to both comply with local environmental discharge levels and facilitate the recycling of wastewater for re-use within the process [2]. In addition to colouration, a number of dye types can be toxic to aquatic ecosystems or human health. In particular azo dyes (consisting of single or multiple azo bonds) are difficult to degrade biologically and are the largest group of textile dyes [3]. While azo dyes themselves are not considered toxic, they can be cleaved under anaerobic conditions if ingested by organisms or microorganisms, forming severely harmful aromatic amines [3–5]. Therefore, their

removal from effluent streams is a critical priority, especially in developing countries where large textile industries are based.

Salt coagulation is often employed for the enmeshment and separation of dyes or other pollutants from wastewater, due to the relatively low cost of the hydrolysing metal salts of aluminium [1,3] or iron [4–7] that are typically used. In order to increase the removal efficiency such that industrial wastewater can be more fully recycled, adsorption can be employed as a secondary step to both increase dye removal and potentially reduce the amount of coagulant required in the process [8–11]. For example, activated carbon is effective as an adsorbent for removal of molecules smaller than the width of the micropores in its structure [10–14], and is frequently used in combined coagulation–adsorption processes [1,10,11]. However, due to slow solute diffusion within the micropores, removal of larger molecular weight compounds such as dyes, adsorption may be limited [12,14] and regeneration of the activated carbon is costly [15] from the high temperatures involved. To this end, low-cost, naturally occurring minerals such as kaolinite [16], zeolite [17] and dolomite [18] have also been previously investigated for dye removal processes [19].

While mineral adsorbents can enhance the removal of pollutants, there are complexities regarding how they are added to the treatment process and combined with other unit operations, in particular for this study, coagulation. For example, large granular media may be incorporated as separate ion exchange units to treat post-coagulated effluent [7,20]. Such systems, however, are inefficient from a material perspective (due to the low surface area to volume ratio) and require considerable plant alterations to retrofit. Additionally, adsorption media may be added in reaction tanks and separated via methods, including flotation [20–22] and membrane filtration [19,20]. Alternatively, a flexible approach that may lead to a number of downstream benefits is to add fine adsorbents directly to coagulation–flocculation operations [23], generating composite flocs that may be separated using sedimentation [7,24,25] or intensified units such as centrifuges [26]. Such approaches will inherently lead to an increase in the sludge mass that must be subsequently separated from the liquid phase. Therefore, the adsorption, coagulation and settling processes must be designed and controlled carefully, so that the permeability, density, compressibility and settling rates of the sludge produced are consistent with low relative volumes [25,27–30].

Continuous stirred-tank reactors (CSTRs) are often used to provide agitation for the coagulation and adsorption stages, due to their simplicity of design. However, they use comparatively high amounts of energy to ensure sufficient dispersion within the tank and require relatively large operational areas [31,32]. Therefore, there has been significant interest in using process intensification to develop new technologies to improve mixing and mass transfer kinetics within chemical reactors, as well as to reduce industrial footprints and energy usage of processing operations [26,33,34]. For example, in-line mixing units using static mixers or jets allow for both a smaller reactor area and a lower coagulant dosage, due to their plug-flow nature [35,36]. Unfortunately, the mixing conditions are complex to model and performance is dependent on the throughput of the unit [35]. Thus, there has also been research into intensified plug-flow reactors where lateral shear and mixing conditions can be altered independently of flowrates. Oscillatory baffle reactors (OBRs) are perhaps the best-known examples of these [33,34], where an oscillatory pump cycle in the range of a few hertz ensures mixing, and bulk throughput rates can be set with a cycle bias. In contrast, this study investigates the use of a novel agitated tube reactor (ATR) for intensified precipitation. The ATR uses a lateral shear generated by a free-floating, mechanically driven agitator bar, which provides almost complete decoupling of the radial mixing shear from reactor throughput [37,38]. Additionally, it is a modular design allowing multiple tubes to be used either in parallel or series within a small operational footprint. The ability of the ATR to act as a combined coagulation–adsorption unit is of interest, as it would allow for efficiency and simplification of the process design, in addition to an easy coupling with downstream intensified separation units.

In summary, the main objectives of this study were to firstly determine the performance of a number of abundant and non-toxic mineral adsorbents for the removal of

common dyes, in combination with hydroxide coagulation, as an inexpensive method to improve treatment performance. Secondly, this study investigated the process intensification of combined coagulation–adsorption operations using a plug-flow reactor. Specifically, the kinetics and equilibrium dye removal rates for five mineral adsorbent materials (treated bentonite, kaolin, talc, calcium carbonate and zeolite) were measured with an anionic azo red dye. The capability of ferric hydroxide coagulant was then assessed as a secondary coagulant, to improve the dye removal efficiency and to alter the physical separation of the adsorbents, where composite settling rates and consolidated sludge volumes were also measured, in bench-scale tests. Finally, the benchmarking of a commercial, pilot-scale ATR was performed to understand its potential as a continuous, pseudo plug-flow coagulation–adsorption unit. Here, the fastest settling coagulated system was selected as a “worst case scenario”, in terms of maintaining adsorbent dispersion along the reactor length.

2. Materials and Methods

2.1. Materials

High-grade, non-toxic mineral samples of bentonite, kaolin, talc, clinoptilolite zeolite and calcium carbonate were provided by Imerys Talc Europe. The bentonite was modified via exchange with a quaternary ammonium chloride cationic surfactant, to increase its capacity for the adsorption of anionic molecules. Previous work by Zhang et al. [39] has shown similar cationic surfactants can embed and expand the interlayer structure of bentonite. The dye used was an anionic dye, Intrabond[®] liquid Scarlet D-BSC (Yorkshire Group, Krefeld, Germany). It is a multiple azo bond-type direct dye with anionic sulphate groups, and similar to the commonly used Fast Scarlet 4BS textile dye [4].

2.2. Batch Adsorption and Coagulation Studies

Mineral equilibrium and kinetic adsorption studies were performed using 1% *w/w* aqueous dispersions of the chosen adsorption materials in 40 mL propylene centrifuge tubes, mixed on a carousel mixer at 100 RPM. Kinetics modelling was performed with a pseudo-second order reaction fit [40] (using MATLAB 2019b, MathWorks Ltd., Cambridge, UK). Residual dye concentrations were measured at 15, 30, 60, 480, 720 and 1440 min for each adsorbent studied.

Batch reactor tests were then performed using an initial concentration of 1% *w/w* adsorbent material in 500 mL conical flasks. The kaolin and zeolite materials were not taken forward for further testing, due to their low dye uptake in the kinetics tests (see Section 3, and the Electronic Supplementary Materials (ESM) for details). Samples were allowed to fully disperse into the solution before adding dye to produce an initial dye concentration of 100 ppm at a mixed volume of 450 mL. The level of dye was chosen to represent a high value for concentration ranges encountered with industrial dye effluents (generally, 10–50 ppm [41–43]). The dispersions were mixed using a magnetic stirrer bar at 300 RPM, to ensure homogeneous mixing was maintained for 15 min.

Further studies were performed utilising iron (III) hydroxide as a coagulant to both enhance the dye removal and increase the adsorbent particle size, and, hence, the settling rate of the final dispersions. For these tests, initial solutions of sodium hydroxide and iron (III) chloride (with a total mixed volume of 50 mL) were added to produce an iron hydroxide coagulant in the dispersion at a final mass concentration of 1% *w/w* (assuming complete reaction). The relative levels of reagents were kept consistent with those reported for the co-precipitation of nuclear effluents [44], although very similar coagulation–precipitation reactions are used commonly in water treatment operations worldwide. For the coagulation studies, the initial mixing time without coagulant was adjusted to 10 min, with an additional 5 min mixing after adding the coagulant chemicals, so that the total mixing time for both sets of experiments was 15 min. A 1% *w/w* excess of sodium hydroxide was used to ensure complete reaction of the iron (III) chloride in the solution. The NaOH was also added before the iron (III) chloride to help prevent an acid-carbonate reaction in the calcium carbonate system. A representation of this procedure is shown in Figure 1.

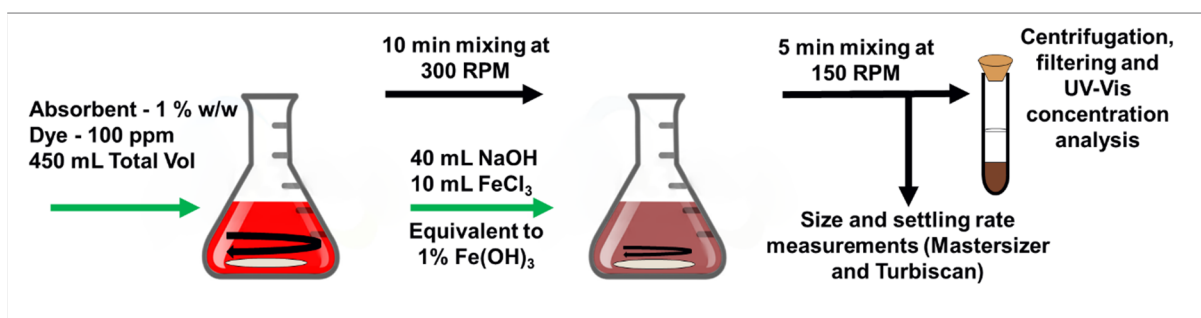


Figure 1. Schematic of the experimental method for combined adsorption and coagulation batch tests.

Residual dye concentration for all systems was measured using a Cary 60 UV–Vis spectrometer (Agilent Technologies, Stockport, UK) at a wavelength of 420 nm, as calibration measurements indicated this provided the best linear fit ($R^2 = 0.999$) between the absorbance and dye concentration in the wavelength spectrum measured (200–800 nm). It gave accurate measurements for changes in dye concentration as low as 0.5 ppm. An example calibration plot for a 420 nm wavelength is shown in the ESM, Figure S1. The selected wavelength was adjusted to 519 nm ($R^2 = 0.996$) with coagulated systems to avoid erroneous results, as there was evidence of dissolved iron that caused peaks close to the 420 nm wavelength. Before the UV–Vis measurements, samples were centrifuged at 12,000 RPM ($RCF/g = \sim 16,100$) using a Heraeus Megafuge16R (Thermo Fisher Scientific, Cheshire, UK) for 5 min, and the supernatant filtered through 200 nm syringe filters to ensure no suspended solids remained in solutions. All measurements were conducted at pH 7 (± 0.1) and 20 °C (± 0.5 °C) and samples were completed in triplicate, to ensure data consistency. The maximum measurement error was assessed by calculating the standard deviation in concentration produced by varying the wavelength used in the UV–Vis spectrometer calibration by 1 nm (around the central wavelength used) to account for bracketing of wavelengths within the spectrometer.

Dispersed and coagulated adsorbent floc sizes, as well as that of the pure iron (III) hydroxide coagulant, were measured using a Mastersizer 2000 (Malvern Panalytical, Malvern, UK). Distributions were averaged over 20 min for coagulated and dispersed adsorbent samples, and over 10 min for pure iron hydroxide.

Floc settling rates were measured using a Turbiscan™ stability analyser (Formulation, Toulouse, France) as undiluted samples in 40 mm glass sample containers. Scanning resolution to determine the interface height was fixed at 1 scan.min⁻¹. The light transmission level, as a function of the sample height over time, was used to find the settling rate.

Scanning electron microscopy and energy dispersive X-ray analysis was performed in an EVO MA15 (Carl Zeiss). Stubs were firstly prepared using samples gently pipetted from the sample container to minimise the shear on the flocs, dried for 12 h and placed under vacuum to remove any trapped water.

2.3. Process Intensification in an ATR

A pilot-scale ATR was modified, utilising a Coflore® ATR (AM Technology, Cheshire, UK) as a method for intensifying the process and reducing the overall plant footprint. It provides strong radial mixing through a perforated metal tube that acts as an internal agitator with minimal axial mixing, allowing for a pseudo plug-flow operation, as described in previous publications [38,45]. A test section (~38 cm long cylinder with an internal volume of 150 mL) was utilised with inlet flow rates and concentrations adjusted to produce residence times identical to those used in batch reactor studies. Direct performance comparisons (dye adsorption capacity, coagulated particle settling rate and final bed volume) were performed between the batch mixer and the ATR flow system.

For the ATR tests, an agitation frequency of 5 Hz was selected, as this has been shown previously to provide ideal sinusoidal movement of the agitator bar to ensure the sediment remains suspended along the length of the reactor [38]. A flow schematic and an image

of the ATR during operation is shown in Figure 2a,b. The concentrated dye solution was introduced through the wider main inlet, while mixed adsorbent dispersions were introduced through a secondary inlet, to prevent the settling of the adsorbent within the tubing during the pumping operation from the low flow rates used ($\sim 11 \text{ mL min}^{-1}$). The overall concentration of the adsorbent in the column was 1% *w/w*, while dye concentration was again 100 ppm (when considering the mixing of both inlet streams together). Calcium carbonate was selected as the adsorbent for the ATR, as it had the largest primary settling rate after coagulation (see Section 3 for details). Therefore, it represented a “worst case scenario” in terms of ensuring sediment suspension along the length of the test section.

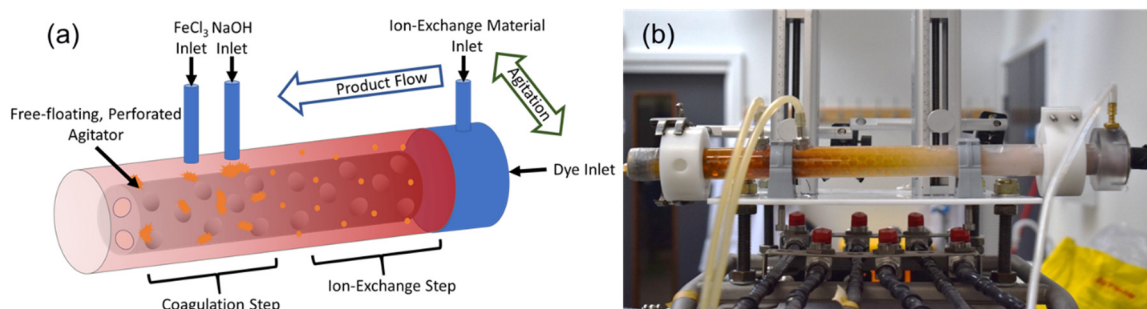


Figure 2. (a) Schematic representation of the ATR and (b) corresponding image of the equipment during operation (same orientation and flow direction).

Sodium hydroxide and iron chloride were introduced via separate inlets approximately 2/3 down the length of the tube (equating to a column residence time period of 10 min). The sodium hydroxide was introduced first to avoid acid–carbonate reactions (see Figure 2a). The composite dye-adsorbent coagulate mixture was then pumped to the outlet of the column, with an equivalent further residence time of 5 min (see image, Figure 2b).

3. Results and Discussion

3.1. Performance of Adsorbents and Physical Characterisation of Composite Coagulate Flocs

Figure 3 shows the pseudo-second order kinetic fits for the anionic dye adsorption process over 500 min with the modified bentonite, talc and calcium carbonate. Here, rate constants of 0.1, 0.07 and 0.44 g/mg.min were found for each adsorbent, respectively. The ESM presents the same data over the full 1500 min of testing, with time presented on a log axis to better differentiate fits in the early time region, see Figure S2. Moreover, presented within the ESM, Table S1, are standard deviations for each measurement as error bars were too small to be visible on the plots shown in Figure 3. First order modelling fits were also produced, but are not shown, as they gave lower values for the correlation coefficient, similar to findings from previous authors [46]. The accuracy of these fits is somewhat limited due to the rapid kinetics observed, although model correlation coefficients were all greater than 0.98. Indeed, it is evident that adsorption values for all systems had almost reached equilibrium within the first 15 min sample time. It was not possible, unfortunately, to reduce the sampling further, because of the time required to centrifuge and separate the supernatant (where the phases are still in contact). However, the results do demonstrate that a 15 min adsorption time would be sufficient for batch reactor tests to achieve residual dye concentration values close to equilibrium. A total of 15 min would also closely reflect a typical hydraulic residence time for an industrial dye adsorption process [47].

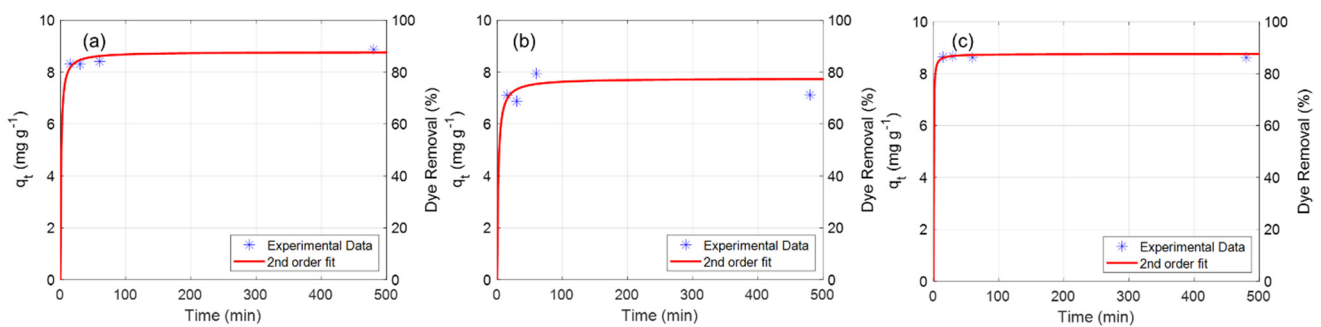


Figure 3. Kinetics of dye uptake with (a) modified bentonite, (b) talc and (c) calcium carbonate using 100 ppm dye solutions over the first 500 min of contact time. Data shown in terms of relative adsorption capacity, q_t (in mg g^{-1}) on left-hand axes, and dye removal percent on right-hand axes.

A final dye uptake from all these three materials in the carousel tests were in the range of 80–90%, for an initial dye concentration 100 ppm. It would be considered, in general, that interactions between the azo dye and the mineral adsorbents would be electrostatic in nature, through the negative sulphate groups to positive mineral surface charges. Apart from the azo groups, the dye contains a few double bonded oxygen and hydroxyl groups [4] although neither would be expected to interact chemically with the mineral surfaces to a significant extent. The high dye adsorption onto calcium carbonate, in particular, can be purely attributed to electrostatic interactions, as calcite is known to have a positive surface charge over a broad pH range [48]. For the bentonite, it is apparent that the surfactant exchange successfully embedded cationic sites into the clay interlayer, again allowing dye adsorption primarily through electrostatic attraction. Indeed, there are no other groups on the surfactant chain tail that would lead to further extensive chemical interactions with the dye (e.g., through hydrogen bonding). The relatively high adsorption onto talc is more surprising (although, it performed the least efficiently of the three) as the overall zeta potential of talc is assumed to be slightly negative [49–51]. However, the surface potential in talc is complex, owing to the presence of both SiOH and MgOH groups on different basal planes [50] where there can be a charge differential on each surface. Additionally, it is known that divalent cations (which may be present as dye counterions, depending on the manufacturing process) can depress the electrostatic charge of talc, or even lead to charge reversal [50,51]. Such interactions have been shown to increase the adsorption of anionic polyelectrolytes onto talc (e.g., carboxymethyl cellulose) where enhanced adsorption may also occur in talc through hydrogen bonding with surface groups [51].

Kinetic results for the kaolin and zeolite samples are shown within the ESM in Figure S3, where they achieved low relative performance (percentage dye uptake < 60% in both cases). The likely reason for the low performance of the zeolite and kaolin is that both are assumed to be highly negatively charged [22,40,52]. Thus, there would be significant electrostatic repulsion to adsorption of an anionic dye. These two materials were, therefore, not considered in further tests.

Figure 4 presents the equilibrium adsorption capacity and percentage dye removal for the modified bentonite, talc and calcium carbonate, where samples were prepared in the 500 mL conical flasks and mixed at 300 RPM for 15 min.

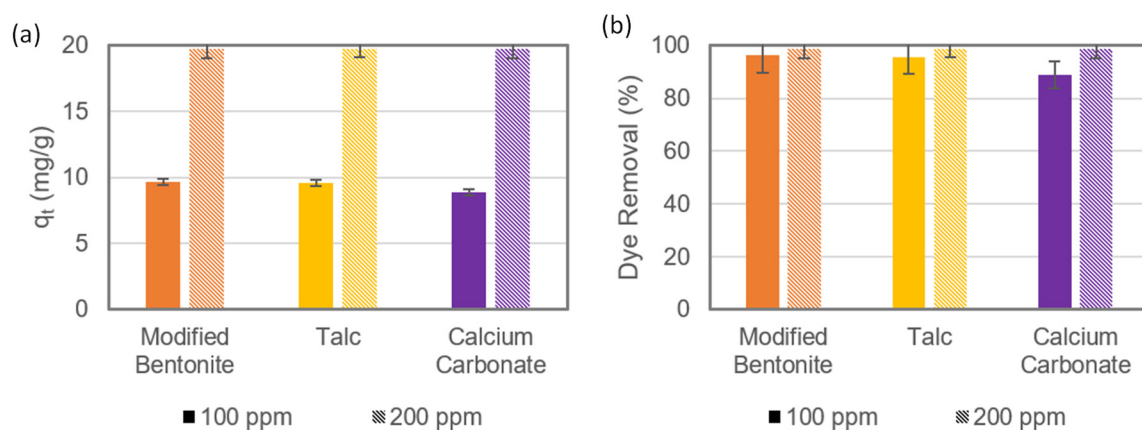


Figure 4. (a) Equilibrium adsorption capacity (q_t) and (b) associated percent uptake of dye with non-coagulated modified bentonite, talc and calcium carbonate after 15 min of mixing in a 500 mL conical flask with 100 and 200 ppm dye solutions.

Results indicate suitably high removal rates in the range of 8.9–9.6 mg g⁻¹ (or ~88–96%) typical of commercial resins used for dye removal [53] at similar concentrations. It is noted that the percentage uptake for all species was slightly higher than observed in the carousel tests (Figure 3) which is attributed to the greater level of dispersion mixing in the conical flasks. Increased removal (19.7–19.8 mg g⁻¹, correlating to 98–99% removal) was observed for 200 ppm dye concentrations in all three materials. It is interesting that the percentage removal was increased for the higher dye concentration, which would not be typical for a small molecule or ion adsorption, due the greater competition for surface sites [40]. Nonetheless, similar enhancements in removal efficiency for higher solute concentrations have been observed previously in studies on textile dye adsorption [54,55] and may be attributed to a greater free energy change of adsorption, leading to a larger osmotic driving force as concentration is increased.

With the performance of the pure adsorbents established, characterisation of their physical properties after coagulation with iron hydroxide was performed. Particle size distributions for each adsorbent studied before and after coagulation are given in Figure 5, where also shown is the size of iron hydroxide flocs without the addition of any adsorbent (in Figure 5a). In all cases, a considerable increase in size upon coagulation is observed, which indicates a good association between the adsorption materials and the coagulant. It would also suggest that the settling rate of the produced composite dispersions should be increased in comparison to the pure materials, because of these larger sizes. Additionally, the minerals should accelerate the sedimentation of the iron hydroxide as well, due to the incorporation of the dense adsorbent into the porous structure of the hydroxide flocs.

Settling curves for the coagulated adsorbent systems, as well as pure iron hydroxide, along with linear fits indicating the zonal settling rate change over time, are presented in Figure 6 (multi-zonal linear fits for all systems are given within the ESM, Figure S4). The highest primary settling rate observed was for the coagulated calcium carbonate system (9.0 mm min⁻¹) which also produced the lowest final bed height of all systems studied. The coagulated talc and modified bentonite systems gave similar primary settling rates (6.5 and 4.9 mm min⁻¹, respectively) with the talc system also having a slightly lower final bed height. All coagulated systems had significantly greater settling rates and bed compression than the pure iron hydroxide, thus, demonstrating the performance enhancing properties of the adsorbents, in terms of the physical separation behaviour of the sludge.

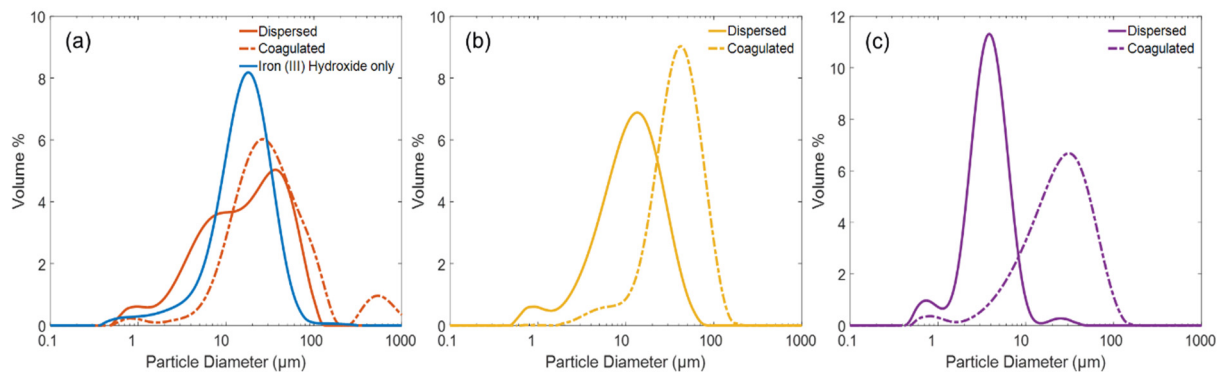


Figure 5. Particle size distributions (PSDs) for (a) modified bentonite, (b) talc and (c) calcium carbonate before and after coagulation with iron hydroxide. PSD for pure iron hydroxide flocs also shown in (a).

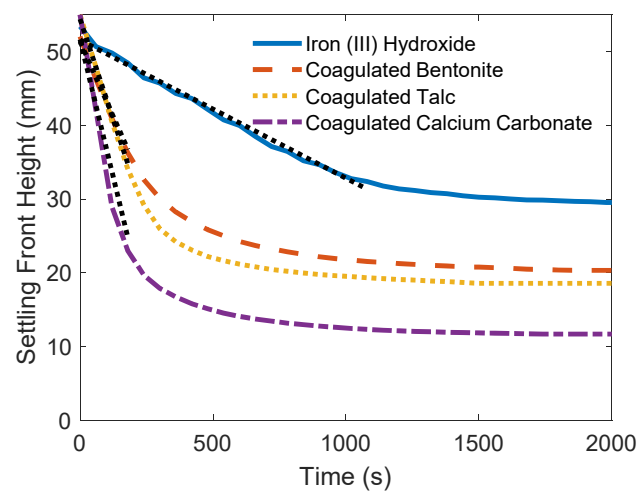


Figure 6. Settling front height versus time for coagulated modified bentonite, talc and calcium carbonate, as well as pure iron hydroxide flocs (dotted black lines indicate fits to obtain settling rates).

Figure 7 presents the primary settling rate of each adsorbent along with the calculated solids volume content of the settled bed. Despite the increase in total mass for the coagulated adsorbent systems (compared to pure iron hydroxide) a higher overall solids loading is achieved in the settled bed, in a much smaller time. Results, therefore, suggest that for an industrial process, considerable increases to throughput or smaller unit operations could be gained through the use of these adsorbents as weighter materials. Figure 8 demonstrates the increase in solids weight fraction as a percentage in the settled bed versus that of the initial dispersion. Data were analysed in terms of percentage changes, due to the fact that the pure iron hydroxide flocs contained only a total of 1% *w/w* solids, while the combined composite coagulants contained 2% *w/w* total solids in the dispersions.

Results for all the coagulated systems studied highlight that a considerably greater density of consolidated bed was produced with the addition of these adsorbents, with the calcium carbonate outperforming the other minerals by almost a factor of two. In general, it is clear that the addition of these weighters would increase the performance of a thickening system, by allowing for a greater compression of the bed, even when taking into account the additional solids loading of the system. Such performance enhancements to both the settling rate and bed compression would markedly reduce the requirement for secondary polymer flocculation. It is also emphasised that all three mineral materials are cost effective, non-toxic and readily available for industrial use, where they will have the additional advantage of acting as dye adsorbents, as well as physical weighters.

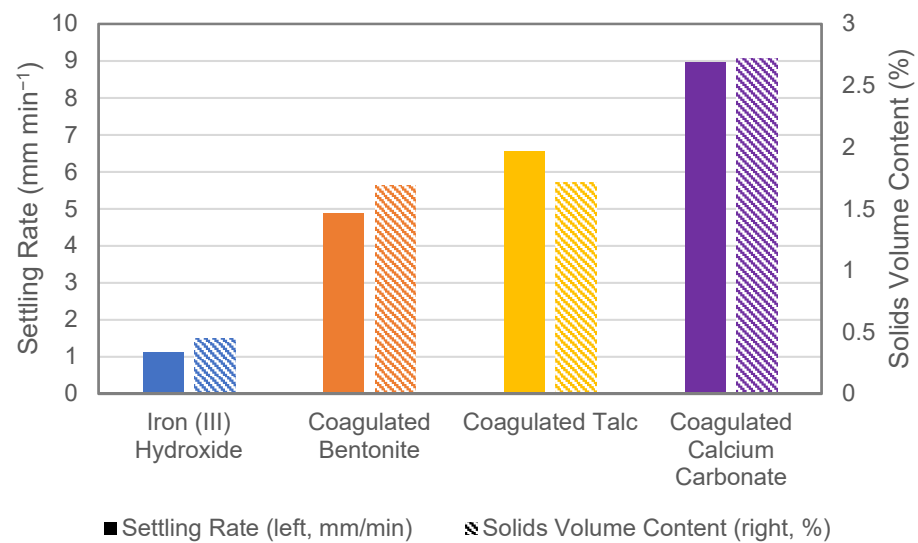


Figure 7. Primary floc settling rates (left-hand axis) and settled bed solids volume content (right-hand axis) for coagulated modified bentonite, talc and calcium carbonate, as well as pure iron hydroxide flocs.

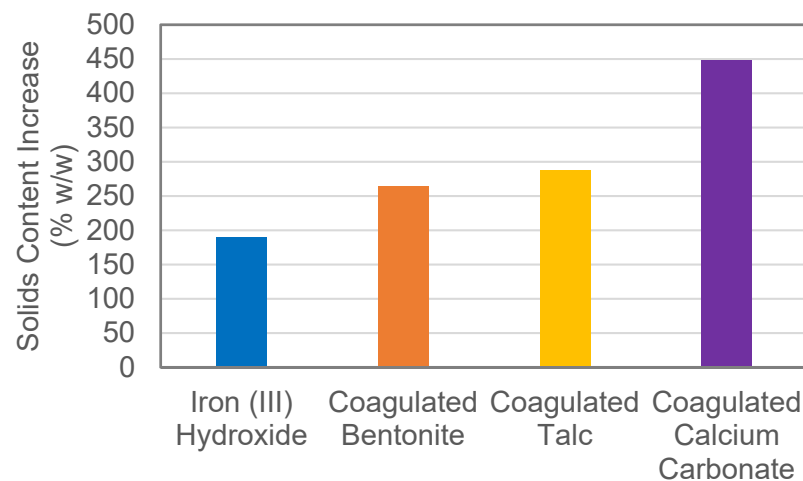


Figure 8. Percentage increase in solids weight fraction from settled coagulated mineral systems, based on consolidated bed density.

3.2. ATR Assessment and Overall Dye Removal Performance

Figure 9 displays images of the ATR taken during operation, as well as a close-up of the outlet flow. While Figure 9a, taken after 20 min of operation, indicates a typical plug-flow system with minimal axial mixing along the length of the reactor, after 90 min of operation (Figure 9b) it became clear that there was some degree of back-mixing of the iron hydroxide coagulant in the test section. The axial mixing observed was caused by a combination of both the high agitation frequency used and the low overall flowrates (11 mL min⁻¹). If multiple agitated tube reactor sections were used in series with angled inlets (which is facilitated by the inherent design of the Coflore[®] ATR) then a greater flow rate could be used. A higher throughput would both reduce the observed axial mixing and allow for a lower agitation frequency, as the additional flow rate would aid the sediment suspension in the reactor. It should also be noted that if an equivalent reactor volume was used while maintaining the same residence time (15 min), the production rate in the ATR would be ~10% higher than for the batch reactor.

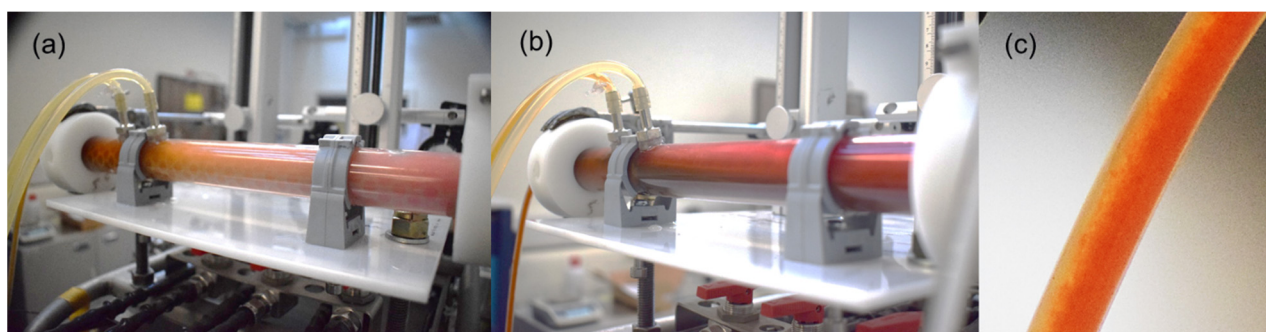


Figure 9. Example images of the agitated tubular reactor during operation at (a) 25 min and (b) 90 min (dye and adsorbent inlets are to the right of each image). Moreover, shown is (c) outlet flow at 90 min.

In Figure 9c which shows the outlet tubing from the ATR, it can be observed that the topside of the tube has a low colour or suspension density (this view is also given as an annotated image in a larger format within the ESM, Figure S5, for clarity). This difference indicates there is some degree of sludge segregation or settling already occurring within the tube once the coagulant dispersion has entered more quiescent conditions. In-line separation could, therefore, be completed between different stages and new feed introduced to reduce the total amount of shear degradation of the coagulated adsorbent, allowing for faster separation. Separation between stages would require more adsorbent material to be used but may increase the overall plant capacity if settling/thickening operations act as a rate limiting step. In-line separation between stages would also allow for the possibility of recycling adsorbent material that has a low dye loading, to earlier stages. Such an operation would enable the adjustment between plug-flow (no recycle) when reactor space is at a premium, and mixed reactor behaviour for situations where the cost of adsorbent materials is high and maximising total adsorption capacity is more cost efficient.

To compare the physical characteristics of the ATR flocs to the batch tests, presented in Figure 10 are the settling and compression data obtained for the ATR samples (the settling curve is given in the ESM, Figure S6, for completeness). It is noted that there is a reduction in both the settling rate and bed solids volume fraction, compared to the batch reactor samples for coagulated calcium carbonate. The reduction in settling rate and bed height is not entirely unexpected, as the large degree of shear generated at the 5 Hz agitation frequency in the ATR is likely to have caused additional breakup of the coagulated adsorbent, thus, decreasing the settling rate of the suspension compared to that seen in the batch reactor tests. In terms of the compression behaviour of the ATR samples, the increase in solids volume content of the samples (Figure 10, right-hand axis) is similar to that of the batch reactor iron hydroxide samples (189% for the ATR sample and 190% for the pure iron hydroxide). Therefore, again there is some loss in the compressibility of the samples in relation to the batch coagulated calcium carbonate. It may be that the final bed compression was not fully achieved within the timescales of the settling experiments, due to the slower settling nature of the coagulated floc. It may also indicate a change in the fractal nature of the aggregates produced by the ATR, due to the plug-flow conditions, with potentially higher levels of bound water. It is known that the coagulation–precipitation of iron hydroxide, or more correctly, iron (oxy)hydroxide (FeOOH) is complex. Initially, largely amorphous phases precipitate out as aggregated colloids (mainly consisting of ferrihydrite [56]) that may crystallise into a number of secondary structures (such as α -FeOOH and β -FeOOH) depending on reagent conditions and aging time [57–59]. Current work is assessing the potential for the ATR to produce differences in the formed oxyhydroxides.

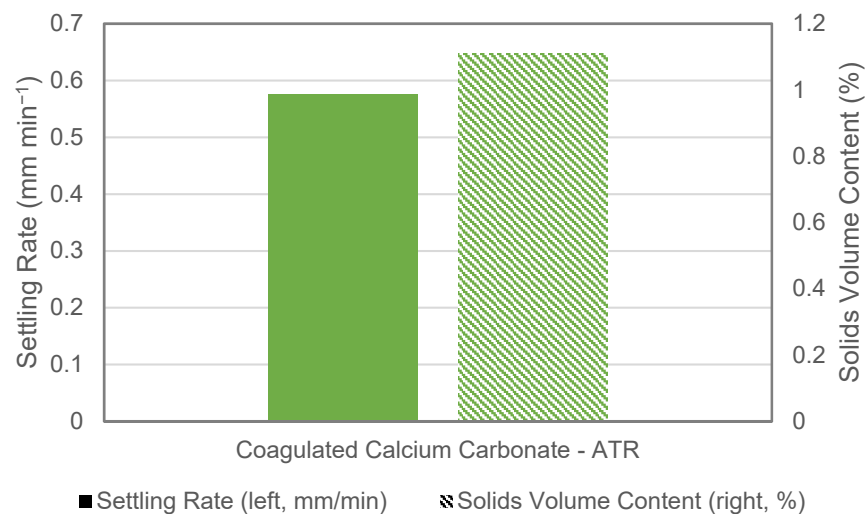


Figure 10. Settling rate (left-hand axis) and increase in solids volume content (right-hand axis) for coagulated calcium carbonate obtained from the ATR after 90 min of operation (using a 15 min reactor residence time).

It is important to consider, however, that the ATR agitation frequency selected (5 Hz) was set at a conservatively high value, to ensure there was no sediment clogging in the reactor. Optimisation of the product (to increase the settling rate and compression) could be easily achieved by adjusting the agitation down to a necessary minimum to ensure good contact between the fluid and adsorbent with minimal sedimentation. Additionally, it would also be possible, as discussed, to redesign the outlet of the reactor to act as an in situ weir to facilitate separation at multiple stages, which would be possible due to the modularity of the system.

In order to demonstrate the physical association between the iron hydroxide coagulant and weighting adsorbent used, Figure 11 shows SEM-EDX images of each coagulated material from batch reactors, as well as a sample taken from the ATR. While it is clear that all adsorbent types make sufficient contact with the coagulant to produce larger particles (as could be inferred from the size data in Figure 5) the calcium carbonate sample had the most even elemental distribution in the iron hydroxide flocs, while the modified bentonite sample presented as fairly heterogeneous. This difference is likely a result of the larger particle size distribution of the bentonite, as compared with talc or the calcium carbonate. These results may also explain the higher settling rates and greater bed densities observed for the talc and calcium carbonate samples, as a more homogenous distribution suggests that the adsorbent may have incorporated iron hydroxide colloidal fines that would otherwise lead to a reduced settling rate. The relatively slower settling observed with the coagulated bentonite may, therefore, be from poorly associated iron hydroxide, decreasing the overall measured hindered settling rate. Additionally, SEM-EDX images of the coagulated samples, obtained from the ATR, also indicate that the ATR provides sufficient mixing to produce similar levels of distribution between the adsorbent and iron hydroxide, when compared to the batch-coagulated calcium carbonate.

With the physical characterisation determined for the coagulated mineral adsorbents, their additional ability to adsorb contaminant dyes was investigated. Figure 12 shows the percentage dye removal in 100 and 200 ppm concentrations from batch tests, for the three minerals with the addition of a coagulant, in comparison to pure iron hydroxide. Moreover, given are results for the coagulated calcium carbonate from the ATR. For nearly all composite coagulated systems, a minimum of 98% removal of the dye was observed. The slightly lower removal percentage seen for the batch-coagulated calcium carbonate system at 100 ppm (94%) can be attributed to a small degree of reaction between the iron (III) chloride and calcium carbonate, which reduced the overall effectiveness of the system, despite pre-mixing the sodium hydroxide in excess before the addition of the iron

(III) chloride. Because iron (III) chloride is a Lewis acid [60] (due to hexaaqua production of acid [61]) and calcium carbonate acts as base in aqueous solutions [62], an acid–base reaction can occur resulting in the production of carbon dioxide [63] and calcium chloride. Additionally, as calcium carbonate has a relatively higher solubility compared to the other minerals used, its potential for reactivity is thought to slightly reduce the adsorption of dye from the solution.

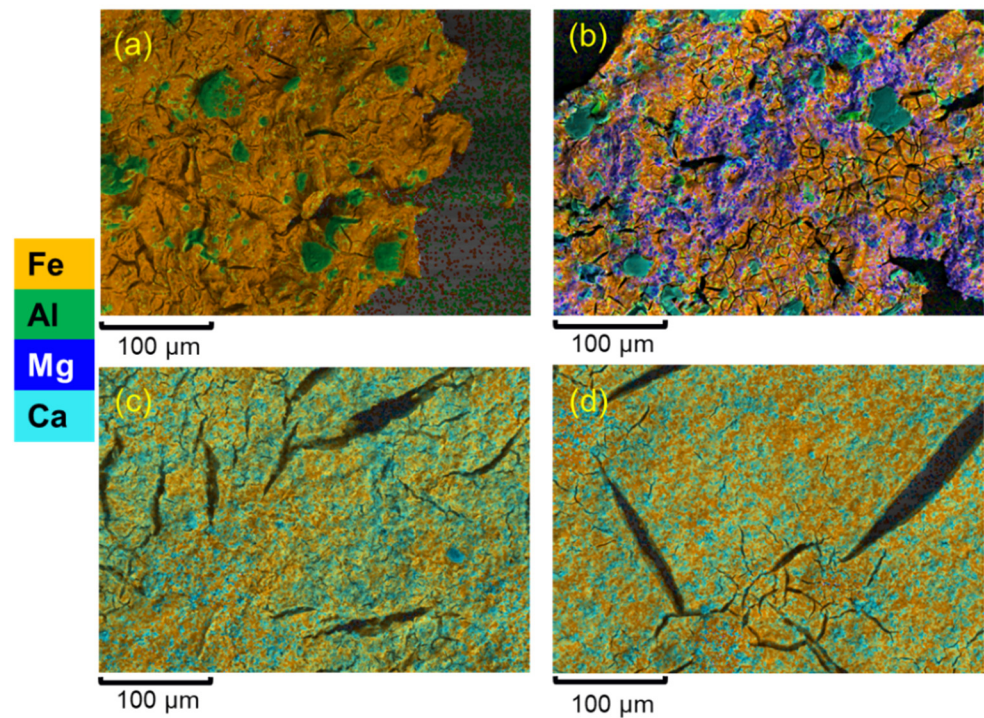


Figure 11. SEM-EDX images of coagulated (a) modified bentonite, (b) talc and (c) calcium carbonate from batch reactor tests, as well as (d) calcium carbonate samples from the ATR.

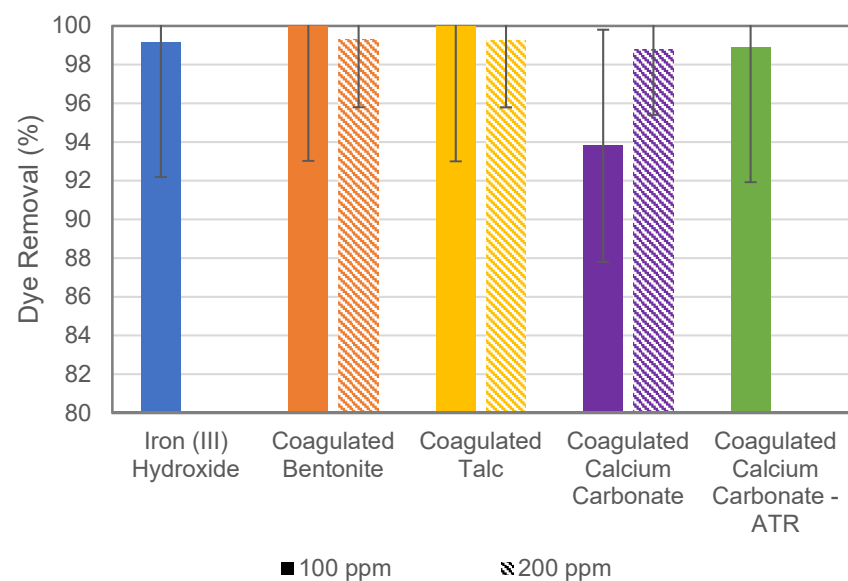


Figure 12. Percentage dye uptake for coagulated modified bentonite, talc and calcium carbonate, in comparison to pure iron hydroxide from batch tests. Moreover, shown is dye uptake for coagulated calcium carbonate from the ATR.

It is noted that the pure iron hydroxide was also seen to remove a high percentage (~99%) of the dye. A previous study by Moghaddam et al. [8] indicated that either charge neutralisation or entrapment of anionic dye molecules by iron hydroxides may be attributed to its high removal capacity. While their study was limited to low pH values, (<5.5) the small excess of sodium hydroxide in this study (1%) would result in final pH values of ~9–10, where iron hydroxide should have a slightly negative zeta potential [64], and, thus, be charge repulsive. Therefore, it appears that in the systems studied here, entrapment of the dye molecules into the coagulated iron hydroxide was the primary mechanism for dye removal. The presence of α -FeOOH, which has been found to be formed in basic solutions of iron hydroxide formed from iron (III) chloride [58,59], may also be contributing to the removal of the anionic dye. FeOOH-treated films have been demonstrated by Liu et al. [9] to remove anionic Congo red dye at 144 mg g^{-1} (where the theoretical maximum was determined to be 2000 mg g^{-1} from their mechanistic study) via a chemisorption mechanism. As the flocs formed in this study will have a large surface area because of their porosity, this may also cause the enhancement in adsorption capacity evidenced here.

In general, the use of the composite coagulated mineral systems is seen to be highly advantageous, as not only do they have the ability to remove additional dye, they also lead to much enhanced separation behaviour, as examined in Section 3.1. In addition, due to the low toxicity of the minerals used, encapsulation of the dye in this manner offers a straightforward route to forward waste processing. While the dye itself does not easily degrade [3], there is evidence that partial breakdown products, such as aromatic amines, can leach into the environment from poorly bound textile and paper solids wastes [65] without appropriate treatment. However, the composite sludges generated in this study, with the dye held by both electrostatic adsorption and co-precipitation entrapment, would serve as a significant barrier to secondary leaching. Such wastes would also be readily accepted in sewage wastewater treatment plants, due to their chemical consistency [57,66], where methods such as Fenton-like processes may further aid biodegradation [67]. Additionally, these wastes are chemically very similar to mine drainage sludges [66], which have been shown to be useful as feedstocks for iron oxide catalysts for enhanced dye removal [68]. The added volume consolidation evident with the mineral adsorbents would also allow easier filtering for disposal as high solids content dried cake wastes [69], which would similarly minimise the potential for chemical leaching.

It is lastly, and importantly, highlighted that the coagulated calcium carbonate from the ATR removed >99% of 100 ppm dye solutions (Figure 12) which is comparatively greater than the efficiency of the calcium carbonate from the batch reactor. The larger degree of agitation present in the ATR may have reduced side reactions, by allowing for a more effective dispersion of the coagulant streams. A reduction in the ratio of calcium carbonate to sodium hydroxide would also reduce the rate of the acid-carbonate reaction, as they are simply parallel reactions in competition. As this results in the production of carbon dioxide gas [63], it would be prudent to include either a gas venting line on the ATR or to angle the outlet so that any gas in the system can be removed. Alternatively, the increase in dye removal may simply be due to the increase in mass transfer rates and mixing efficiency, or smaller residence time distributions, from the plug-flow dynamics. Indeed, previous modelling of the ATR has shown relatively high levels of viscous energy dissipation [38] while it has also led to enhancements in mass transfer when used as an intensified ion exchange column [45].

4. Conclusions

This study investigated the integrated use of various mineral adsorbents and iron (oxy)hydroxide ('FeOOH') as composite coagulants to remove anionic azo red dye. Trials were conducted in both batch reactors and an intensified continuous ATR. Three non-coagulated minerals (talc, calcite and modified bentonite) were able to remove 90–95% of dye at 100 and 200 ppm concentrations, where the kinetics were fitted to a pseudo second-

order rate model, and observed adsorption was rapid (<30 min). Adsorption was mostly attributed to electrostatic effects, although surface interactions were considered to be more complex in the case of talc, with the potential for hydrogen bonding to occur. In secondary coagulation testing, the particle size distributions of all composite mineral-FeOOH systems were significantly larger than the bare minerals or FeOOH coagulant alone, leading to rapid settling rates, especially in the case of calcium carbonate. Critically also, not only were the settling rates enhanced, but solids consolidation was improved, showing up to a 450% increase in the solids fraction of the settled beds for the composite systems. SEM-EDX data also provided additional evidence that the minerals were evenly dispersed throughout the coagulated FeOOH matrix, especially in the case of calcium carbonate. Collectively, results indicated that these minerals could be used as cost-effective dual-function weighter materials, aiding both dye removal and physical separation of the sludge.

The benchmarking performed using the ATR indicated dye removal was slightly enhanced with respect to that observed for the batch reactor tests using calcium carbonate, where the performance was attributed to an increase in mass transfer efficiency from the plug-flow design or reduction of side reactions. Nonetheless, the resulting settling rate of the final product was lower than observed for the batch reactor with the same material, which was attributed to the conservatively high agitation rate (5 Hz) used to ensure sediment suspension. Using higher flow rates and optimising inlet pipe angles could allow for lower agitation rates to be used to maintain suspension, while producing larger floc sizes and settling rates. Additionally, there is a trade-off between required residence times for complete precipitation against the degree of agitation and product settling rate that warrants further investigation. Regardless of this compromise, the ATR overall presents the opportunity to enhance operational efficiency and flexibility between a plug-flow and mixed reactor system, while it can lead to an increased production rate compared to an equivalent volume CSTR. It is also noted that as the device contains up to 10 tubes that can be run in parallel, the reactor could be scaled-up with a minimal footprint increase in a modular fashion and, thus, it may offer significant advantages if used as a mobile system for industrial effluent treatment or waste clean-up.

Supplementary Materials: The following are available online at <https://www.mdpi.com/article/10.3390/chemengineering5030035/s1>, Figure S1: (a) UV-Vis spectrum data (200–800 nm) for azo dye at 1–100 ppm, with a (b) concentration calibration and (c) low-concentration region showing the lower limit of detection. Figure S2: Kinetics of dye uptake with (a) modified bentonite, (b) talc and (c) calcium carbonate using 100 ppm dye solutions over 1500 min on a logarithmic scale. Figure S3: Kinetics results for dye uptake with (a) kaolin and (b) zeolite. Figure S4: Settling curves for coagulated adsorbents; (a) modified bentonite, (b) talc and (c) calcium carbonate. Moreover, shown is (d) iron hydroxide floc only. Figure S5: Annotated image of outlet flow from the agitated tube reactor after 90 min of operation. Figure S6: Settling curve for coagulated calcium carbonate samples obtained from the ATR after 90 min of operation (using a 15 min reactor residence time). Table S1: Standard deviation in q_t (mg g^{-1}) for dye uptake kinetic data.

Author Contributions: Individual contributions to the paper are as follows: Conceptualization, T.N.H., D.H., S.C. and C.C.; Methodology, T.N.H., D.H., S.C., M.Z. and C.C.; Formal analysis, A.S.T., T.N.H., S.C. and M.Z.; Investigation, A.S.T. and T.N.H.; Resources, T.N.H., D.H., S.C., M.Z. and C.C.; Data curation, A.S.T.; Writing—original draft preparation, A.S.T.; Writing—reviewing and editing, T.N.H., D.H., S.C., M.Z. and C.C.; Supervision, T.N.H., D.H., S.C., M.Z. and C.C.; Project administration, T.N.H. and S.C.; Funding acquisition, T.N.H., D.H. and S.C. All authors have read and agreed to the published version of the manuscript.

Funding: This project was funded by the Engineering and Physical Sciences Research Council (EPSRC) UK, University of Leeds and Imerys, France, under an Impact Acceleration Account (EP/R511717/1).

Data Availability Statement: Additional supporting data is available on request.

Acknowledgments: The authors thank the listed agencies (EPSRC, University of Leeds, Imerys) for project funding. John Harrington and the Leeds Electron Microscopy and Spectroscopy (LEMAS) centre is thanked for their support with the SEM-EDX. We would also like to gratefully acknowledge Robert Ash and AM Technology for project support and the use of the pilot-scale Coflore® ATR.

Conflicts of Interest: We wish to confirm that there are no known conflicts of interest associated with this publication, and there was no significant financial support for this work that could have influenced its outcome, apart from the grant funding listed in the funding and acknowledgements.

References

1. Furlan, F.R.; de Melo da Silva, L.G.; Morgado, A.F.; de Souza, A.A.U.; Guelli Ulson de Souza, S.M.A. Removal of reactive dyes from aqueous solutions using combined coagulation/flocculation and adsorption on activated carbon. *Resour. Conserv. Recycl.* **2010**, *54*, 283–290. [[CrossRef](#)]
2. Holkar, C.R.; Jadhav, A.J.; Pinjari, D.V.; Mahamuni, N.M.; Pandit, A.B. A critical review on textile wastewater treatments: Possible approaches. *J. Environ. Manag.* **2016**, *182*, 351–366. [[CrossRef](#)] [[PubMed](#)]
3. Li, J.-T.; Li, M.; Li, J.-H.; Sun, H.-W. Decolorization of azo dye direct scarlet 4BS solution using exfoliated graphite under ultrasonic irradiation. *Ultrason. Sonochem.* **2007**, *14*, 241–245. [[CrossRef](#)] [[PubMed](#)]
4. Sun, W.; Sun, W.; Wang, Y. Biosorption of Direct Fast Scarlet 4BS from aqueous solution using the green-tide-causing marine algae *Enteromorpha prolifera*. *Spectrochim. Acta Part A Mol. Biomol. Spectrosc.* **2019**, *223*, 117347. [[CrossRef](#)] [[PubMed](#)]
5. Afshari, M.; Dinari, M. Synthesis of new imine-linked covalent organic framework as high efficient absorbent and monitoring the removal of direct fast scarlet 4BS textile dye based on mobile phone colorimetric platform. *J. Hazard. Mater.* **2020**, *385*, 121514. [[CrossRef](#)] [[PubMed](#)]
6. Puchana-Rosero, M.; Lima, E.; Mella, B.; Costa, D.; Poll, E.; Gutterres, M. A coagulation-flocculation process combined with adsorption using activated carbon obtained from sludge for dye removal from tannery wastewater. *J. Chil. Chem. Soc.* **2018**, *63*, 3867–3874. [[CrossRef](#)]
7. Lin, S.H.; Chen, M.L. Purification of textile wastewater effluents by a combined Fenton process and ion exchange. *Desalination* **1997**, *109*, 121–130. [[CrossRef](#)]
8. Sadri Moghaddam, S.; Alavi Moghaddam, M.R.; Arami, M. Coagulation/flocculation process for dye removal using sludge from water treatment plant: Optimization through response surface methodology. *J. Hazard. Mater.* **2010**, *175*, 651–657. [[CrossRef](#)]
9. Liu, J.; Wong, L.M.; Wong, L.H.; Chiam, S.Y.; Li, S.F.Y.; Ren, Y. Immobilization of dye pollutants on iron hydroxide coated substrates: Kinetics, efficiency and the adsorption mechanism. *J. Mater. Chem. A* **2016**, *4*, 13280–13288. [[CrossRef](#)]
10. Papić, S.; Koprivanac, N.; Lončarić Božić, A.; Meteš, A. Removal of some reactive dyes from synthetic wastewater by combined Al(III) coagulation/carbon adsorption process. *Dyes Pigment.* **2004**, *62*, 291–298. [[CrossRef](#)]
11. Lee, J.-W.; Choi, S.-P.; Thiruvenkatachari, R.; Shim, W.-G.; Moon, H. Evaluation of the performance of adsorption and coagulation processes for the maximum removal of reactive dyes. *Dyes Pigment.* **2006**, *69*, 196–203. [[CrossRef](#)]
12. Galán, J.; Rodríguez, A.; Gómez, J.M.; Allen, S.J.; Walker, G.M. Reactive dye adsorption onto a novel mesoporous carbon. *Chem. Eng. J.* **2013**, *219*, 62–68. [[CrossRef](#)]
13. Lorenc-Grabowska, E.; Gryglewicz, G.; Gryglewicz, S. Development of mesoporosity in activated carbons via coal modification using Ca- and Fe-exchange. *Microporous Mesoporous Mater.* **2004**, *76*, 193–201. [[CrossRef](#)]
14. Derylo-Marczewska, A.; Marczewski, A.W.; Winter, S.; Sternik, D. Studies of adsorption equilibria and kinetics in the systems: Aqueous solution of dyes–mesoporous carbons. *Appl. Surf. Sci.* **2010**, *256*, 5164–5170. [[CrossRef](#)]
15. Ge, X.; Wu, Z.; Cravotto, G.; Manzoli, M.; Cintas, P.; Wu, Z. Cork wastewater purification in a cooperative flocculation/adsorption process with microwave-regenerated activated carbon. *J. Hazard. Mater.* **2018**, *360*, 412–419. [[CrossRef](#)]
16. Harris, R.G.; Wells, J.D.; Johnson, B.B. Selective adsorption of dyes and other organic molecules to kaolinite and oxide surfaces. *Colloids Surf. A Physicochem. Eng. Asp.* **2001**, *180*, 131–140. [[CrossRef](#)]
17. Armağan, B.; Turan, M.; Elik, M.S. Equilibrium studies on the adsorption of reactive azo dyes into zeolite. *Desalination* **2004**, *170*, 33–39. [[CrossRef](#)]
18. Walker, G.M.; Hansen, L.; Hanna, J.-A.; Allen, S.J. Kinetics of a reactive dye adsorption onto dolomitic sorbents. *Water Res.* **2003**, *37*, 2081–2089. [[CrossRef](#)]
19. Crini, G. Non-conventional low-cost adsorbents for dye removal: A review. *Bioresour. Technol.* **2006**, *97*, 1061–1085. [[CrossRef](#)]
20. Solmaz, S.K.A.; Üstün, G.E.; Birgül, A.; Taşdemir, Y. Treatability studies with chemical precipitation and ion exchange for an organized industrial district (OID) effluent in Bursa, Turkey. *Desalination* **2007**, *217*, 301–312. [[CrossRef](#)]
21. Younker, J.M.; Walsh, M.E. Bench-scale investigation of an integrated adsorption–coagulation–dissolved air flotation process for produced water treatment. *J. Environ. Chem. Eng.* **2014**, *2*, 692–697. [[CrossRef](#)]
22. Prajitno, M.Y.; Tangparitkul, S.; Zhang, H.; Harbottle, D.; Hunter, T.N. The effect of cationic surfactants on improving natural clinoptilolite for the flotation of cesium. *J. Hazard. Mater.* **2021**, *402*, 123567. [[CrossRef](#)]
23. Bu, F.; Zhou, W.; Yue, Q.; Liu, C.; Wang, W.; Shen, X. The Combination of Coagulation and Adsorption for Controlling Ultra-Filtration Membrane Fouling in Water Treatment. *Water* **2019**, *11*, 90. [[CrossRef](#)]
24. Ahmad, A.L.; Ismail, S.; Bhatia, S. Optimization of coagulation-flocculation process for palm oil mill effluent using response surface methodology. *Environ. Sci. Technol.* **2005**, *39*, 2828–2834. [[CrossRef](#)]

25. Yuan, Y.; Wen, Y.; Li, X.; Luo, S. Treatment of wastewater from dye manufacturing industry by coagulation. *J. Zhejiang Univ. Sci. A* **2006**, *7*, 340–344. [[CrossRef](#)]
26. Seyfang, B.C.; Klein, A.; Grützner, T. Extraction Centrifuges—Intensified Equipment Facilitating Modular and Flexible Plant Concepts. *ChemEngineering* **2019**, *3*, 17. [[CrossRef](#)]
27. Hunter, T.N.; Peakall, J.; Egarr, D.; Cowell, D.M.J.; Freear, S.; Tonge, A.S.; Horton, L.; Rice, H.P.; Smith, I.; Malone, K.; et al. Concentration profiling of a horizontal sedimentation tank utilising a bespoke acoustic backscatter array and CFD simulations. *Chem. Eng. Sci.* **2020**, *218*, 115560. [[CrossRef](#)]
28. Usher, S.P.; Spehar, R.; Scales, P.J. Theoretical analysis of aggregate densification: Impact on thickener performance. *Chem. Eng. J.* **2009**, *151*, 202–208. [[CrossRef](#)]
29. Scales, P.J.; Kumar, A.; van Deventer, B.B.G.; Stickland, A.D.; Usher, S.P. Compressional dewatering of flocculated mineral suspensions. *Can. J. Chem. Eng.* **2014**, *93*, 549–552. [[CrossRef](#)]
30. Wei, H.; Gao, B.; Ren, J.; Li, A.; Yang, H. Coagulation/flocculation in dewatering of sludge: A review. *Water Res.* **2018**, *143*, 608–631. [[CrossRef](#)]
31. Sun, Y.; Zhou, S.; Chiang, P.-C.; Shah, K.J. Evaluation and optimization of enhanced coagulation process: Water and energy nexus. *Water-Energy Nexus* **2019**, *2*, 25–36. [[CrossRef](#)]
32. Ghernaout, D.; Boucherit, A. Review of Coagulation's Rapid Mixing for NOM Removal. *J. Res. Dev. Chem.* **2015**, *2015*, 1–32. [[CrossRef](#)]
33. Coward, T.; Tribe, H.; Harvey, A.P. Opportunities for process intensification in the UK water industry: A review. *J. Water Process Eng.* **2018**, *21*, 116–126. [[CrossRef](#)]
34. Wang, H.; Mustaffar, A.; Phan, A.N.; Zivkovic, V.; Reay, D.; Law, R.; Boodhoo, K. A review of process intensification applied to solids handling. *Chem. Eng. Process. Process Intensif.* **2017**, *118*, 78–107. [[CrossRef](#)]
35. Lang, J.S. Treatment Plant Operations: Optimize Initial Mixing with Plug-Flow Reactors. *Opflow* **2002**, *28*, 12–22. [[CrossRef](#)]
36. Jones, S.C.; Amirtharajah, A.; Sotiropoulos, F.; Skeens, B.M. *Using Static Mixers to Mix Coagulants: CFD Modeling and Pilot-Plant Experiments BT-Chemical Water and Wastewater Treatment VI.*; Hahn, H.H., Hoffmann, E., Ødegaard, H., Eds.; Springer: Berlin/Heidelberg, Germany, 2000; pp. 79–88.
37. Derksen, J.J. Mixing in an agitated tubular reactor. *Can. J. Chem. Eng.* **2019**, *97*, 523–527. [[CrossRef](#)]
38. He, Y.; Bayly, A.E.; Hassanpour, A.; Fairweather, M.; Muller, F. Flow behaviour of an agitated tubular reactor using a novel dynamic mesh based CFD model. *Chem. Eng. Sci.* **2020**, *212*, 115333. [[CrossRef](#)]
39. Zhang, H.; Kim, Y.K.; Hunter, T.N.; Brown, A.P.; Lee, J.W.; Harbottle, D. Organically modified clay with potassium copper hexacyanoferrate for enhanced Cs⁺ adsorption capacity and selective recovery by flotation. *J. Mater. Chem. A* **2017**, *5*, 15130–15143. [[CrossRef](#)]
40. Prajitno, M.Y.; Harbottle, D.; Hondow, N.; Zhang, H.; Hunter, T.N. The effect of pre-activation and milling on improving natural clinoptilolite for ion exchange of cesium and strontium. *J. Environ. Chem. Eng.* **2020**, *8*, 102991. [[CrossRef](#)]
41. Laing, I.G. The impact of effluent regulations on the dyeing industry. *Rev. Prog. Color. Relat. Top.* **1991**, *21*, 56–71. [[CrossRef](#)]
42. Shelley, T.R. Dye pollution clean-up by synthetic mineral. *Int. Dye.* **1994**, *79*, 26–31.
43. Pierce, J. Colour in textile effluents—The origins of the problem. *J. Soc. Dye. Colour.* **1994**, *110*, 131–133. [[CrossRef](#)]
44. Hildred, K.; Townson, P.; Hutson, G.; Williams, R. Characterisation of particulates in the BNFL Enhanced Actinide Removal Plant. *Powder Technol.* **2000**, *108*, 164–172. [[CrossRef](#)]
45. Prajitno, M.Y.; Taufiqurrakhman, M.; Harbottle, D.; Hunter, T.N. Kinetic studies of Cs⁺ and Sr²⁺ ion exchange using clinoptilolite in static columns and an agitated tubular reactor (ATR). *ChemEngineering* **2021**, *5*, 9. [[CrossRef](#)]
46. Simonin, J.-P. On the comparison of pseudo-first order and pseudo-second order rate laws in the modeling of adsorption kinetics. *Chem. Eng. J.* **2016**, *300*, 254–263. [[CrossRef](#)]
47. Boyer, T.H. Removal of Dissolved Organic Matter by Magnetic Ion Exchange Resin. *Curr. Pollut. Rep.* **2015**, *1*, 142–154. [[CrossRef](#)]
48. Elliott, L.N.; Bourne, R.A.; Hassanpour, A.; Edwards, J.L.; Sutcliffe, S.; Hunter, T.N. Salt enhanced solvent relaxation and particle surface area determination via rapid spin-lattice NMR. *Powder Technol.* **2018**, *333*, 458–467. [[CrossRef](#)]
49. Wang, X.; Liu, R.; Ma, L.; Qin, W.; Jiao, F. Depression mechanism of the zinc sulfate and sodium carbonate combined inhibitor on talc. *Colloids Surf. A Physicochem. Eng. Asp.* **2016**, *501*, 92–97. [[CrossRef](#)]
50. Bremmell, K.E.; Addai-Mensah, J. Interfacial-chemistry mediated behavior of colloidal talc dispersions. *J. Colloid Interface Sci.* **2005**, *283*, 385–391. [[CrossRef](#)]
51. Jin, S.; Shi, Q.; Li, Q.; Ou, L.; Ouyang, K. Effect of calcium ionic concentrations on the adsorption of carboxymethyl cellulose onto talc surface: Flotation, adsorption and AFM imaging study. *Powder Technol.* **2018**, *331*, 155–161. [[CrossRef](#)]
52. Zhang, H.; Tangparitkul, S.; Hendry, B.; Harper, J.; Kim, Y.K.; Hunter, T.N.; Lee, J.W.; Harbottle, D. Selective separation of cesium contaminated clays from pristine clays by flotation. *Chem. Eng. J.* **2019**, *355*, 797–804. [[CrossRef](#)]
53. Wawrzkievicz, M. Anion Exchange Resins as Effective Sorbents for Removal of Acid, Reactive, and Direct Dyes from Textile Wastewaters. In *Ion Exchange: Studies and Applications*; Kilislioglu, Z.H.E.-A., Ed.; IntechOpen: Rijeka, Croatia, 2015.
54. Wawrzkievicz, M. Anion Exchange Resins as Effective Sorbents for Acidic Dye Removal from Aqueous Solutions and Wastewaters. *Solvent Extr. Ion Exch.* **2012**, *30*, 507–523. [[CrossRef](#)]
55. Robinson, T.; Chandran, B.; Nigam, P. Removal of dyes from a synthetic textile dye effluent by biosorption on apple pomace and wheat straw. *Water Res.* **2002**, *36*, 2824–2830. [[CrossRef](#)]

56. Weatherill, J.S.; Morris, K.; Bots, P.; Stawski, T.M.; Janssen, A.; Abrahamsen, L.; Blackham, R.; Shaw, S. Ferrihydrite Formation: The Role of Fe13 Keggin Clusters. *Environ. Sci. Technol.* **2016**, *50*, 9333–9342. [[CrossRef](#)]
57. Salehin, S.; kumar Kulandaivelu, J.; Rebosura, M.; van der Kolk, O.; Keller, J.; Doederer, K.; Gernjak, W.; Donose, B.C.; Yuan, Z.; Pikaar, I. Effects of aging of ferric-based drinking water sludge on its reactivity for sulfide and phosphate removal. *Water Res.* **2020**, *184*, 116179. [[CrossRef](#)] [[PubMed](#)]
58. Tanaka, H.; Miyafuji, A.; Kandori, K.; Ishikawa, T.; Nakayama, T. Effect of Cu(II) on the formation, morphology and molecular adsorption properties of α -FeOOH rust particles prepared from acidic Fe(III) solutions. *Corros. Sci.* **2013**, *66*, 337–342. [[CrossRef](#)]
59. Ristić, M.; Opačak, I.; Štajdohar, J.; Musić, S. The influence of CTAB and gum arabic on the precipitation of α -FeOOH in a highly alkaline medium. *J. Mol. Struct.* **2015**, *1090*, 129–137. [[CrossRef](#)]
60. Miles, W.H.; Nutaitis, C.F.; Anderton, C.A. Iron(III) Chloride as a Lewis Acid in the Friedel-Crafts Acylation Reaction. *J. Chem. Educ.* **1996**, *73*, 272. [[CrossRef](#)]
61. Hock, S. *Precipitation of Hematite and Recovery of Hydrochloric Acid from Aqueous Iron(II, III) Chloride Solutions by Hydrothermal Processing*; Department of Mining and Materials Engineering, McGill University: Montreal, QC, Canada, 2009.
62. Rouchon, V.; Belhadj, O. Calcium Hydrogen Carbonate (Bicarbonate) Deacidification. *J. Pap. Conserv.* **2016**, *17*, 125–127. [[CrossRef](#)]
63. Williams, B.B.; Gidley, J.L.; Guin, J.A.; Schechter, R.S. Characterization of Liquid-Solid Reactions. Hydrochloric Acid-Calcium Carbonate Reaction. *Ind. Eng. Chem. Fundam.* **1970**, *9*, 589–596. [[CrossRef](#)]
64. Lay, M.-L.; Wu, H.-M.; Huang, C.-H. Study of the zeta potential of Fe(O)OH colloids. *J. Mater. Sci.* **1995**, *30*, 5473–5478. [[CrossRef](#)]
65. Ning, X.-A.; Liang, J.-Y.; Li, R.-J.; Hong, Z.; Wang, Y.-J.; Chang, K.-L.; Zhang, Y.P.; Yang, Z.-Y. Aromatic amine contents, component distributions and risk assessment in sludge from 10 textile-dyeing plants. *Chemosphere* **2015**, *134*, 367–373. [[CrossRef](#)]
66. Rakotonimaro, T.V.; Neculita, C.M.; Bussière, B.; Benzaazoua, M.; Zagury, G.J. Recovery and reuse of sludge from active and passive treatment of mine drainage-impacted waters: A review. *Environ. Sci. Pollut. Res.* **2017**, *24*, 73–91. [[CrossRef](#)] [[PubMed](#)]
67. Zou, H.; Ning, X.-A.; Wang, Y.; Zhou, F. The agricultural use potential of the detoxified textile dyeing sludge by integrated Ultrasound/Fenton-like process: A comparative study. *Ecotoxicol. Environ. Saf.* **2019**, *172*, 26–32. [[CrossRef](#)] [[PubMed](#)]
68. Flores, R.G.; Andersen, L.F.; Maia, L.K.K.; José, H.J.; Moreira, R.d.F.P.M. Recovery of iron oxides from acid mine drainage and their application as adsorbent or catalyst. *J. Environ. Man.* **2012**, *111*, 53–60. [[CrossRef](#)]
69. Mahdi, F.M.; Hunter, T.N.; Holdich, R.G. A study of cake filtration parameters using the constant rate process. *Processes* **2019**, *7*, 746. [[CrossRef](#)]